Available online at www.sciencedirect.com

ScienceDirect

journal homepage: www.elsevier.com/locate/issn/15375110

Research Paper

Modeling and simulation of creep response of sorghum stems: Towards an understanding of stem geometrical and material variations

Omid Zargar, Matt Pharr, Anastasia Muliana *

Department of Mechanical Engineering, Texas A&M University, USA

ARTICLE INFO

Article history:
Received 4 October 2021
Received in revised form
9 January 2022
Accepted 15 February 2022

Keywords:
Sorghum
Stem lodging
Biomechanical response
Creep
Viscoelasticity
Specimen morphologies

Sorghum [*Sorghum bicolor (L.)*] is a tropical grass that often suffers from structural failure (lodging) when subjected to wind, rain, and hail. During lodging, excessive lateral deflection occurs, which inherently correlates with the biomechanical properties of the stem. As such, a fundamental understanding of sorghum's biomechanical behavior is required to mitigate its propensity for lodging. Herein, we perform creep tests to characterize the mechanical behavior of Della genotype sorghum stems and their constituents, i.e., their rind and pith. This study also examines the influence of various testing geometries and boundary conditions on mechanical property characterization. We determine that small geometric irregularities typical of sorghum stems (e.g., from straight circular cylinders) do not affect their mechanical response in an overall engineering strain sense. However, these typical geometric irregularities do lead to nonuniform (localized) stresses and strains, thereby influencing the quantification of certain properties during mechanical testing. We also implement a viscoelastic constitutive model to describe the creep responses of the individual constituents (rind and pith), as to predict the overall biomechanical response of the stems. We find that even though the rind carries most of the load in the stem and itself does not show a significant time-dependent response, an overall time-dependent response of the stem still occurs, arising from viscoelastic effects in the pith.

1. Introduction

Cereal crops (e.g., sorghum, corn, rice, etc.) are susceptible to lodging when exposed to dynamic forces from wind, rain, hail, etc. Lodging is associated with excessive lateral displacements (bending) of plant stems which disrupt their growth and development, and can further lead to stem breaking (stem lodging) and/or anchorage failure (root lodging). Dwarf varieties were widely used during the Green Revolution era to minimize lodging from mechanical forces, which significantly improved cereal crop yields. However, with global climate changes and an increase in crop yields, the dwarf varieties have become less effective, and the frequency of lodging has increased (Berry et al., 2004; Hirano et al., 2017; Niu et al., 2016). In the past ten years, efforts in mitigating lodging in rice, wheat, sorghum, and maize have shifted to the understanding of the biomechanics of stems with the intention to

* *Corresponding author.*
E-mail address: amuliana@tamu.edu (A. Muliana).
https://doi.org/10.1016/j.biosystemseng.2022.02.009

develop new lodging-resistant variants (Berry et al., 2004; Hirano et al., 2017).

The biomechanical behavior of plants has been widely investigated, mainly regarding their elastic properties, through experimentation (Gomez, Carvalho, et al., 2018a; Gomez, Muliana, & Rooney, 2018b; Robertson et al., 2017; Robertson et al., 2015). However, testing of these plants presents challenges in terms of proper characterization relative to standard engineering materials. As an example, in standard uniaxial compression tests, a straight cylindrical specimen is often used. However, plants grow with irregular shapes that deviate from simple geometries (e.g., perfect straight cylindrical sections). To the best of our knowledge, no standardized tests exist specifically for fresh (live) plant tissues, which are complex composite systems and often of small size. A few standards have been reported for lumber and wood materials (ASTM-D4761, Standard test methods for mechanical properties of lumber and wood-based structural material) but these standards are not always applicable to soft plant tissues. The lack of specific standards leads to difficulties in extracting useful comparable information from different sources in literature, particularly in tests on fresh plant stems, which have large contents of water. In conducting tensile testing of fresh stems, gripping presents challenges as slippage often occurs in the grip area; these effects are less problematic in the testing of dry hollow stems (Wright et al., 2005; Zeng et al., 2015). During compression tests, misalignment between the samples and fixtures (e.g., compression platens) will result in nonuniform stress distributions and even buckling and/or rotating of the samples due to geometric variation in both the cross-sectional and longitudinal directions. Using self-aligning compression platens can partially mitigate this issue (Al-Zube et al., 2017), but challenges remain in properly determining the material properties from the raw load–displacement test outputs.

Most experimental studies have focused on determining elastic properties and failure behaviors under bending, tension, and compression (Al-Zube et al., 2017; Gomez et al., 2017; Kin & Shim, 2010; Lemloh et al., 2014; Robertson et al., 2015; Wright et al., 2005). However, plant tissues (dry or wet) show viscoelastic responses and exhibit microstructural reconfigurations due to mechanical loadings. Thus, further experimental investigation on creep/viscoelastic and permanent deformation is of interest. To this end, researchers have used a dead weight on living plants (in vivo) or plants submerged in water (in vitro) to conduct creep tests, in which custom-built extensometers equipped with linear displacement transducers can measure elastic, viscoelastic, and plastic deformations (Alméras et al., 2002; Edelmann & Köhler, 1995; Ulrich Kutschera & Briggs, 1987, 1988; U Kutschera & Schopfer, 1986; Robertson et al., 2017; Suslov & Verbelen, 2006). Recently, Lee. et al. (Lee et al., 2020) have conducted uniaxial compression tests on fresh sorghum stems. They have found that sweet sorghum stems exhibit significant time-dependent mechanical responses, owing to both viscoelastic and poroelastic behavior. These time-dependent responses have important ramifications in stem lodging under dynamic forces of various frequencies (e.g., due to wind).

As plant stems comprise hierarchical structures with different microstructural morphologies and constituent responses, geometric features, including cross-sectional shapes and dimensions, can affect the stress distribution in the stems and cause early failure in some regions (D. U. Shah, T. P. Reynolds, & M. H. Ramage, 2017). Additionally, the mechanical properties of the individual pith and rind constituents together produce the overall mechanical responses of the stem. Wirawan et al. (Wirawan et al., 2011) have shown that the elastic and viscoelastic properties of sugarcane composites are correlated with the fiber content of pith and rind. Robertson et al. (2017) and Stubbs et al. (Stubbs et al., 2018) have shown that rind tissues are load-bearing components in terms of longitudinal stresses produced by bending in thin-walled plant stems. In another work, Al. Zube. et al. (Al-Zube et al., 2017) have demonstrated that the contribution of the pith tissue within maize stems affects the compressive modulus of the stems; moreover, the presence of the pith tissues prevents the stems from buckling and hence contributes to the overall strength of the stems (Zuber et al., 1980). Likewise, understanding the influence of morpho-anatomical and biomechanical properties of tissues and cell components on the overall plant behaviors often relies on modeling and simulation. Cisse et al. (Cisse et al., 2015) modeled the tensile creep tests of hemp fibers using an anisotropic constitutive model developed by (Boubakar et al., 2003) to capture the long-term viscoelastic behavior. The model is based on rheological models, e.g., generalized Kelvin-Voigt and Maxwell models. They have revealed that single hemp fibers show significant delayed and large permanent strain due to loading and unloading, respectively, which originates from instantaneous and time-dependent mechanisms. Recently, Song and Muliana (Song & Muliana, 2019) proposed a constitutive material model to capture the creep tensile behavior of plant stems, considering microstructural changes in stems during loading. They have incorporated the effects of microstructural changes of plant networks on overall macroscopic mechanical behaviors using a multiple natural configuration method, which was formulated and successfully implemented to describe responses of soft materials (De Tommasi et al., 2006; Yuan et al., 2020).

In this study, we investigate the biomechanical responses of sorghum stems, particularly their viscoelastic responses. There are currently no standardized testing methods for characterizing the biomechanical properties of plant stems, as pointed out by (Shah et al., 2017); instead, testing methods commonly used for engineering materials have been adopted for testing plant stems. Difficulties in testing plant stems arise from variability and complexity of the geometrical shapes of the stems, unlike in engineering materials where sample size and shape can be readily controlled. To aid in addressing this issue, herein we investigate the effects of geometrical characteristics of plant stems, different material properties of the constituents (pith and rind), and boundary conditions in the experimental tests on the overall biomechanical behavior. Specifically, we examine the sorghum [*Sorghum bicolor (L.)*] Della genotype, as grown in a greenhouse. We conduct experimental creep tests under uniaxial compression on sorghum stems and pith, and tests under uniaxial tension on the rind and pith. We then perform finite element (FE) simulations of sorghum stems to better understand the influence of the variabilities in geometries and boundary conditions on the

stems' mechanical response during experimental testing. This "virtual testing" can aid in characterizing the properties of plant stems and their constituents through mimicking real experiments. As such, we first evaluate the influence of stem cross-sectional and longitudinal nonuniformities on the overall creep response. We then study the effects of different creep responses of the individual constituents (rind and pith) on the overall behavior of the stems.

2. Materials and methods

2.1. Plant material

One group of sorghum cultivar Della was selected for tensile creep testing and another for compression creep testing. They were planted in February and April 2019, respectively, in the Borlaug Center greenhouse located at 30.6° N in College Station, TX. Plants were grown in 19 L pots containing a fine sandy loam soil amended with 14–14-14 slow-release fertilizer. The greenhouse temperature was 26–30 °C day/21–26 °C night, and the photoperiod was 14 h day/10 h night, with supplemental light provided by high-pressure sodium lamps. Each group was harvested for mechanical testing at grain maturity, approximately 13 weeks after planting.

2.2. Sample preparation

Plants were harvested for mechanical testing by cutting the stems at the soil level. All sorghum samples were collected in the morning before temperatures increased (8–10 AM), as to minimize the amount of water lost through evapotranspiration. All tests were performed within 6 h after cutting the internode from the plant. Internode numbers were counted based on the first elongated internode above the ground to the last internode below the peduncle. For uniaxial tensile tests, the pith and rind specimens were cut into thin plate samples; while for the uniaxial compression tests the pith and the stem were cut into cylindrical shapes. The information regarding the type of testing, internode number, and sample sizes are categorized in Table 1.

2.3. Creep testing on stems and their constituents

Uniaxial creep tests were conducted on the stems and their constituents (pith and rind) using an Instron 5943 with a 1 kN load cell for 1 h at ~50% of the strength as measured from quasi-static ramp tests (at a loading rate of 1/min). All tests were performed at room temperature, ~23 °C. A rigid test platen was implemented for the compression tests (Lee et al., 2020). In this setup, some lateral deformations can also occur at the top and bottom surfaces of the specimens, as they were not fixed (i.e., glued) to the platen (See Fig. 1a-b). For the tensile tests, blocks were used to hold the specimens, with dimensions based on the sample thickness, to provide fixed boundary conditions and to avoid slippage issues at the grips (See Fig. 1c-d). The samples were glued to the blocks using Loctite Super Glue (Al-Zube et al., 2018). The axial stress was calculated by dividing the measured force by the initial cross-sectional area of the specimens. The compressive specimens had a circular cross-section, while the tensile specimens had a rectangular cross-section. Compressive tests were performed on the entire stem and pith tissues, while tensile tests were performed on its constituents (pith and rind tissues). The strain was calculated by dividing the displacement of jaw fixtures by the initial distance between the grips (blocks). These quantities represent nominal "engineering" stress and strain values of homogenized materials from ideal specimens (perfectly straight and circular cross-section). As discussed above, plant tissues are composites of complex geometries that experience non-uniform stress and strain fields within the specimens. Herein, we perform finite element simulations to explore the influence of non-uniform stress and strain fields, geometric and material variations, and testing boundary conditions on the overall quantification of the creep responses during experiments.

2.4. 3D finite element (FE) modeling of the stems

To simulate creep responses of plant stems, a linear viscoelastic material model for isotropic materials was considered and implemented using a UMAT subroutine in ABAQUS FE software. The isotropic material was adopted due to limited available data since we only measured the uniaxial responses in the experiments. If sufficient experimental data existed to capture the anisotropic and nonlinear viscoelastic response of the plant stems and their constituents (rind, pith), a nonlinear viscoelastic model for anisotropic materials (e.g., Sawant and Muliana (Sawant & Muliana, 2008), Song and Muliana (Song & Muliana, 2019)) could be used. To examine the implications of isotropic and anisotropic mechanical properties of stem tissues on the overall uniaxial and bending responses of plant stems, we performed simulations as discussed in Appendix A. It is seen that the effect of transversely isotropic properties on the uniaxial response relevant for the experimental test conducted is negligible. It is also seen that the transversely isotropic tissue properties have a negligible effect on the bending responses. The results are expected since under uniaxial loading and bending the deformations are mostly governed by the material responses along the longitudinal

Table 1 – Testing type, internode number, and plant constituent anatomical properties.

Type of Test	Internode Number	Plant Constituent	Dimensions (mm)			
			Diameter	Length	Thickness	Width
Compression Creep (Lee et al., 2020)	9 & 10	Pith	10.5–10.7	13.2–14.5	–	–
		Stem	11.6–12.1	18.5–18.7	–	–
Tensile Creep	3, 4, 5 & 6	Pith	–	73.4–107	1.37–2.77	2.81–6.36
		Rind	–	70.5–81.5	0.19–0.66	2.84–4.49

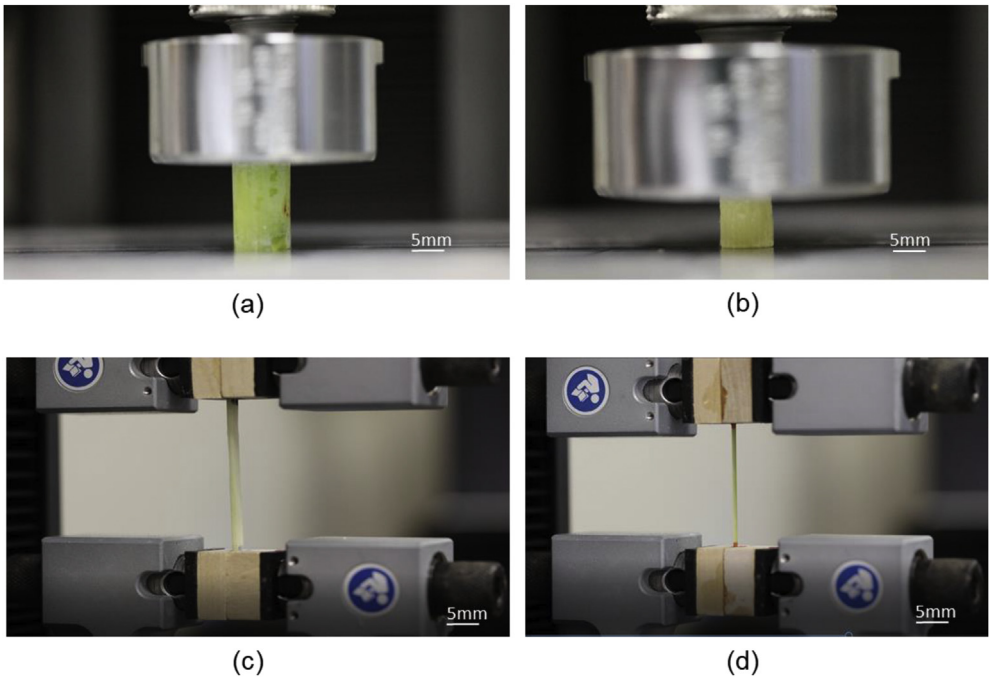

Fig. 1 – Experimental set-up for (a) creep compression loading of a section of a stem, (b) creep compression loading of a section of pith, (c) tensile creep loading of a section of pith, and (d) tensile creep loading of a section of rind.

(axial) axis of the specimens. The linear viscoelastic model is expressed in terms of the deviatoric and volumetric strain components:

$$\varepsilon_{ij}(t) = \frac{1}{2}\int_{0^-}^{t} J(t-s)\frac{dS_{ij}(s)}{ds}ds + \frac{1}{3}\delta_{ij}\int_{0^-}^{t} B(t-s)\frac{d\sigma_{kk}(s)}{ds}ds \quad (1)$$

where $S_{ij}(t) = \sigma_{ij}(t) - \frac{1}{3}\delta_{ij}\sigma_{kk}(t)$ is the deviatoric stress component, $\sigma_{kk}(t)$ is the volumetric stress component, and δ_{ij} is the Kronecker delta. The shear and bulk creep compliances are given as $J(t) = 2(1+\nu_o)D(t)$ and $B(t) = 3(1-2\nu_o)D(t)$, respectively, where ν_o is a Poisson's ratio, which is assumed constant, and $D(t)$ is the extensional creep compliance, given as:

$$D(t) = \left(\frac{1}{E_0} + \sum_{i=1}^{N}\frac{1}{E_i}\left(1-e^{\frac{-t}{\tau_i}}\right)\right) \quad (2)$$

where E_o is the instantaneous elastic modulus, N is the number of Prony terms, and E_i and $\tau_i$are the time-dependent parameters to be used in the viscoelastic material model and the relaxation time, respectively, for each Prony term. The reason for using the Prony series for the memory kernel is due to its numerical advantage, in which the integral in Eq. (1) can be solved recursively, thereby reducing the computational cost. The disadvantage of using the memory kernel in Eq. (2) is due to its large number of material parameters required to capture the creep response. In addition, in the Prony series there is no uniqueness in the material parameters, where it is possible to have different combinations of characteristic times and weighting factors to fit the creep data. In this study, we started by picking the characteristic times in Table 2 and then calibrated the parameters E_i by fitting the creep data. It is possible to pick slightly different characteristic times, as long as they are within the range of experimental data, and recalibrate the parameters E_i.

Table 2 – Instantaneous moduli and time-dependent parameters of sorghum stem under creep compression loading (E_1 to E_5 are time-dependent parameters to be used in a viscoelastic material model).

i	τ_i(s)	E_i (MPa)
0	–	54.0
1	5	582.8
2	50	317.8
3	500	569.3
4	5000	638.0
5	50,000	141.9

The stems were first simulated as perfect cylinders to extract the overall stress–strain responses, treating them as a homogenized body. For compression loading, two types of boundary conditions were chosen for the models while we applied pressure to the top surface: (1) free lateral sliding at the top and bottom surfaces and (2) fixed conditions at the top and bottom surfaces. For tensile testing, we considered fixed conditions at both ends. For the compression and tension simulations, the model was meshed using three-dimensional 8-node hexahedral linear brick (solid) elements. We also performed four-point bending simulations in which the model was meshed using three-dimensional 20-node hexahedral quadratic brick (solid) elements. Generally speaking, the stem specimens are not perfect cylinders, so simulations were performed to investigate the influence of the actual stem geometries, as measured from real plants through optical images, on the mechanical response. Simulations were also conducted to study how the properties of the individual rind and pith

constituents contribute to the overall mechanical response, i.e., as compared to treating the stem as a homogeneous body.

2.5. Data analysis

Experimental data were extracted using the Instron software (Bluehill® Universal 4.01) and processed in Microsoft Excel thereafter. Material properties were calibrated using the curve fitting tool in Matlab® software and then imported in ABAQUS/CAE 2018. To calculate the 'elastic moduli' of the specimens, the initial slopes under tensile and compression tests were calculated from 0 to 0.5% (linear range) after implementing a toe correction method (Lee et al., 2020).

3. Results

In Sections 3.1–3.4, we explore the effect of geometric characteristics and boundary conditions on the measured creep responses of sorghum stems. For this purpose, we considered creep responses from compression testing of stems. In Sections 3.5–3.7, we elucidate the influence of different responses of pith and rind on the overall creep responses of stems under compression, tension, and bending.

3.1. Mesh size convergence study from creep compression of a perfect cylinder

A mesh size study was carried out for a simple perfect cylinder (11.92 mm in diameter and 18.67 mm in height) to evaluate the stability of the finite element method. We considered fixed boundary conditions at the top and bottom surfaces for the stem while applying a 1.9 MPa pressure load on the top surface. Based on Fig. 2, it can be seen that the von Mises stress converges (plateaus) above ~3000 elements. Specifically, using 3382 elements with an average element edge length of 1 mm is an optimal mesh size.

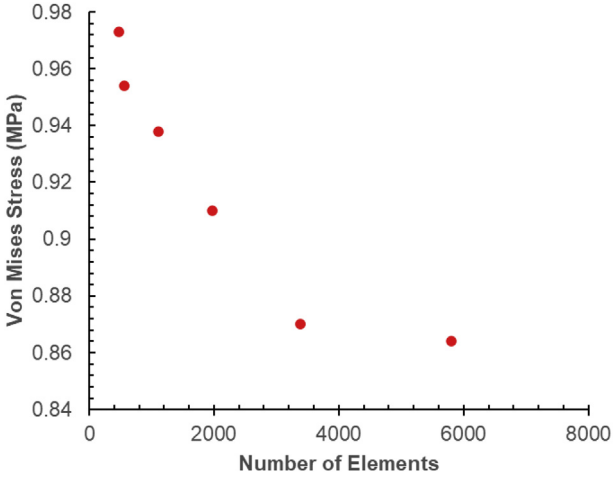

Fig. 2 – Results from a mesh-size convergence study from creep compression simulations of a perfect cylinder. The von Mises stress reported is at the center of the bottom surface of the stem. The stress converges (plateaus) above ~3000 elements.

3.2. Calibration of material parameters from creep compression testing of stems

The experimental data we used for calibrating material parameters from the compression creep responses represent the average response from three experimental creep tests of sorghum stems from our previous study (Lee et al., 2020). The elastic 'instantaneous moduli' of the specimens was calculated using the initial slopes under compression tests from 0 to 0.5% strain (linear range). Since we only extract the axial response in the experiments, we do not measure Poisson's ratio. As such, we use a typical value of 0.25 for the Poisson's ratio in the simulations (Stubbs et al., 2018). The time-dependent parameters for the stem were calibrated from experimental data (see Table 2). An applied stress of 1.9 MPa, which was used in the experiment, was prescribed to the model. Figure 3 shows the creep response from the experimental data and model from the material calibration. In conducting the calibration from the uniaxial compression data, the sorghum stem was treated as a homogenized body.

The stem was first modeled as a perfect cylinder, 11.92 mm in diameter and 18.67 mm in height. In our finite element analysis, we consider two boundary conditions that represent the limits of investigating lateral deformation effects between the compression platen and the sample. One boundary condition represents free sliding in the lateral direction, and the other boundary condition represents no sliding (full constraint) in the lateral direction. For modeling the free sliding condition, the top and bottom surfaces of the sample are constrained to uniformly move in the axial direction and are allowed to expand or contract in the lateral direction. In this condition, the axial displacement field is uniform. The overall "engineering strain" determined from the simulations with the two boundary conditions are nearly identical, and they are comparable to experimental results (Fig. 3). For the fully constrained boundary conditions where we allow the sample to undergo bulging, strain localization occurs in the specimen, and hence the displacement field varies through the sample (see Fig. 4). These variations in strain fields through the specimen can influence material parameter calibrations, as the overall "engineering strain" measure does not necessarily represent the local strain field in the experiment. During our actual experiments, the boundary condition on the top and bottom surfaces of the specimen is somewhere between the free sliding and fully constrained limits.

3.3. Effects of non-circular cross-sections on compressive creep response of stems

In this section, we investigate the effects of typical cross-sectional variations found among plants on extracting the overall engineering stress–strain behavior from experiments. Generally speaking, the stem dimensions and hence the distribution of the cross-section (shape) through the height of the sample might affect the overall response. Since we obtained an optical image from the top of the plant, for simplification, we focus on the top surface of the sample and assume that the cross-section maintains its shape through the height of the sample. The total number of elements in the analysis was 3116. As before, we considered two different boundary

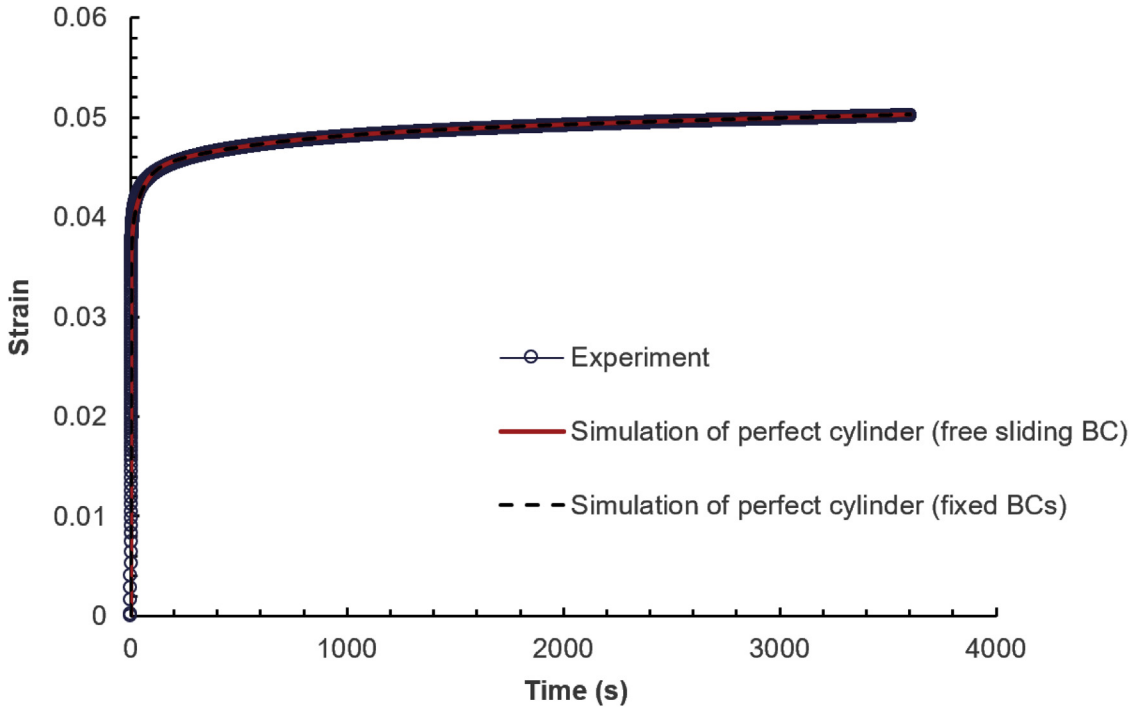

Fig. 3 – Modelling a perfect cylinder under creep compression loading of 1.9 MPa while considering free sliding and fixed boundary conditions.

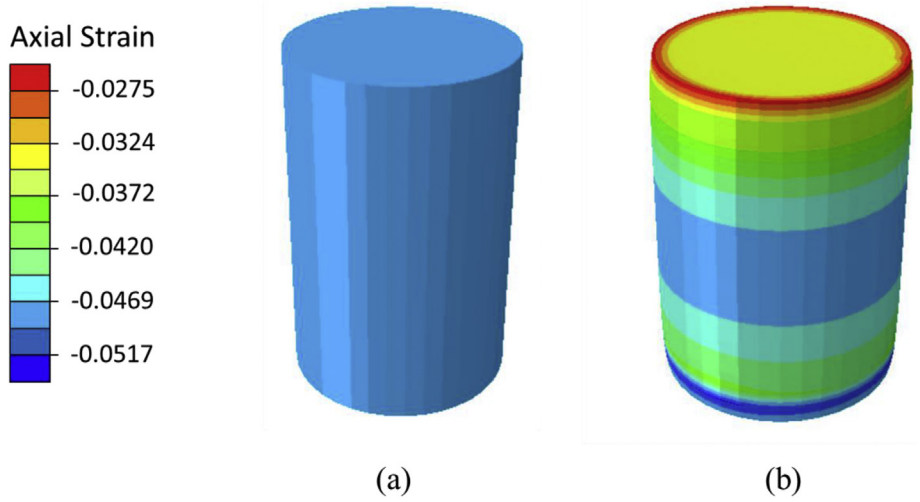

Fig. 4 – Axial strain contour plot for a simple cylinder model under creep compression at t = 1000 s for (a) free sliding boundary condition and (b) fixed boundary condition.

conditions: one of free sliding at the sample/platen interfaces, as to allow free lateral deformation, and the other of constraining the lateral displacement of the sample at the sample/platen interface. The result for free sliding at the platen interface is shown in Fig. 5. Based on Fig. 5, we can see there is no change in the overall engineering strain output compared to the one from the simple cylinder model, which indicates that the cross-sectional variation does not significantly affect the overall axial deformation of the stem. For the fixed boundary conditions at the top/bottom surfaces, a spatial variation occurs in the displacement field; strain localization changes the strain response by 17% at the bottom of the sample and 49% at the top of the sample, as compared to the simple straight cylinder (percent difference) (Fig. 6).

3.4. *Effect of non-straight specimens on the creep compression response*

In this section, we use FE analysis to study the effect of samples that are not perfectly straight (along their long axis), which is common in plant stems, on extracting the overall engineering stress–strain behavior from mechanical testing. In reconstructing a real specimen, around 3 degrees of misalignment between the plant and the normal to the top/

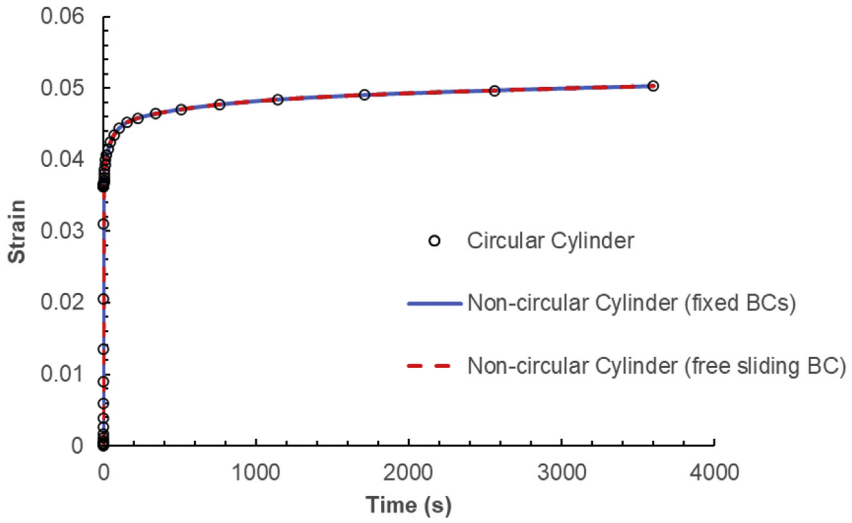

Fig. 5 – Overall response during creep compression with free-sliding boundary conditions of a "real" cylinder with a non-circular cross-section.

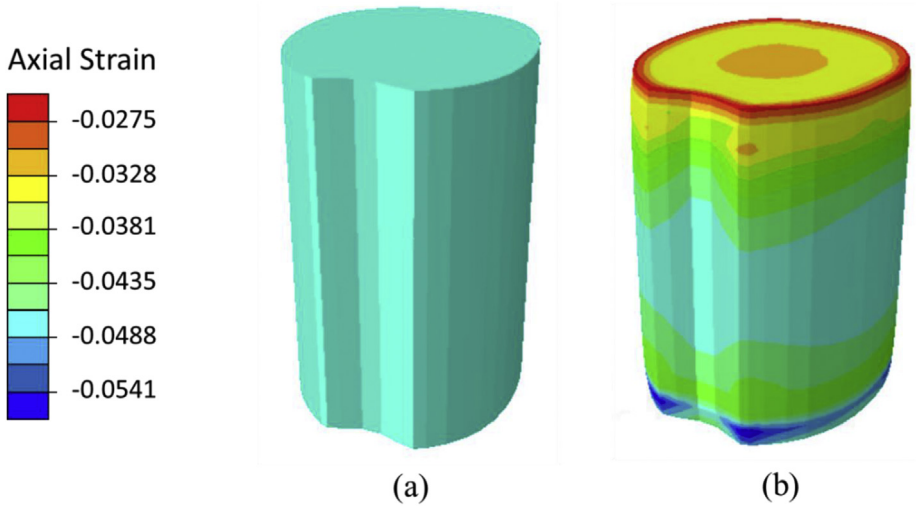

Fig. 6 – Axial strain contour plot of a "real" cylinder with non-circular cross-section under creep compression loading at time t = 1000 s for (a) free sliding boundary condition and (b) fixed boundary condition.

bottom surfaces was found to be typical in real plants (Fig. 7). The total number of elements in the analysis was 8175. Again, we considered the two boundary conditions as previously described. The strain field is seen in Fig. 7 for both the free sliding boundary condition (Fig. 7a) and the fixed boundary condition (Fig. 7b) for the realistic geometry. Strain localization occurs within the sample where the axial strain varies between 29% and 32% (relative percent difference) for the free sliding boundary condition and varies between 35% and 51% (relative percent difference) for the fixed boundary condition, as compared to the simple straight cylinder. The strain localization is due to the misalignment of the stem leading to bending and thus localized regions of tension and compression, even though the overall "engineering strain" through the dimension of the sample was found to be equivalent to the experimental data we have collected. Figure 8a shows the strain output at specific locations of the stem as indicated in Fig. 7 for the free sliding boundary condition, which indicates strain localization in certain regions. Likewise, Fig. 8b shows strain localization at corresponding locations of the stem for the fully constrained boundary condition. The strain measure determined from the experiments is based on the overall displacement (d/L, the "engineering strain"), while strains are field variables that can vary throughout the specimens. A large variation in strain response of Node A, B, and C can be also seen between the free sliding and fixed boundary conditions: 33%, 5.3%, and 6.3% (relative percent difference), respectively.

3.5. *Effects of different properties of the constituents (rind and pith) on compression creep tests*

We next studied the influence of different properties of the individual constituents (rind and pith) on the overall creep

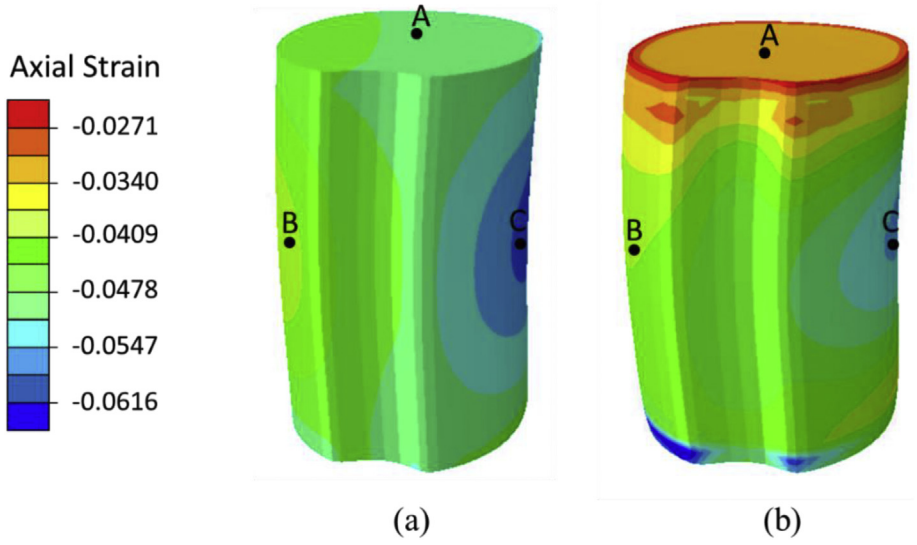

Fig. 7 – Axial strain contour plot of a "real" stem with an axial misalignment through the height (non-straight) under creep compression loading for a) free sliding and b) fixed boundary conditions at time t = 1000 s.

compression of stems. Experimental tests were conducted on the pith tissue under creep compression. However, the rind is relatively thin, which made it impossible to do compression tests without inducing buckling. Comparing the pith and stem compressive responses (Lee et al., 2020), it is seen that the stems are much stiffer and stronger than the pith. We thus conclude that the stiffness and strength of the stems are largely due to the stiffer and stronger rind. Since the rind is quite stiff and does not exhibit significant creep compared to the pith (shown in the next section), we modeled the rind as linear elastic. For the pith, we calibrated time-dependent properties from creep compression tests (Table 3). The pith specimens were obtained from the same internodes as the stem specimens. Using FE simulations to match the instantaneous strain for the overall displacement (d/L) and the experiment, the elastic modulus of the rind was calibrated as approximately 325 MPa. Figure 9a shows the strain field within the stem with an elastic rind and a viscoelastic pith with a fixed boundary condition at the bottom surface. To mimic the compression experiment, a pressure is applied at the top surface of the rigid platen which is in contact with the sample (See Fig. 9b). The contact between the platen and the sample was defined as a surface to surface contact interaction with a finite-sliding formulation and a hard penalty pressure–overclosure relationship considering tangential friction with a coefficient of friction of 0.2. The total number of elements for the stem in the analysis was 6840. Figure 10 shows the variation of strain locally within the stem. The creep response of the pith constituent is also included for comparison. These results indicate that the overall engineering strain obtained from the simulation (d/L) can capture the experimental creep responses.

3.6. *Simulating tension responses*

We now analyze the influence of tension responses of the individual constituents (rind and pith) on the overall tension behavior of the stem. The pith and rind properties were calibrated and shown in Tables 4 and 5, respectively. The internode length and diameter were measured as 102 mm and 11.9 mm, respectively, and the thickness of the rind was measured as 0.62 mm. As mentioned in previous studies distinguishing between the rind and pith is somewhat challenging, as the boundaries are not distinct (Stubbs et al., 2019). Herein we identified the boundaries using optical images of the stem cross-section simply by considering rind as dark green tissue and pith as a light green region through the RGB color analyzer (using a threshold for light green and dark green), as to estimate the thickness of the rind. The elastic moduli for the pith and rind were calibrated as 20 MPa and 580 MPa, respectively. The creep stress levels (defined as the stress at 50% of the strength) for pith and rind were 0.8 MPa and 18.5 MPa, respectively. The stem was assumed to be fixed at both ends while we apply external tensile loading at the top surface. In the simulations, we use external stress of 1.1 MPa to ensure that the produced stress in the pith constituent is smaller than the strength of the pith (1.6 MPa). Three different geometries were modeled. Figure 11a–11c shows the strain contours in a straight cylinder with a non-circular cross-section (A), a non-circular cylinder with a single curvature through the height (B), and a non-circular cylinder with two curvatures through the height (C). The total number of elements for the non-circular straight cylinder, non-circular cylinder with a single curvature, and non-circular cylinder with two curvatures was 21,012, 13,940, and 11,135, respectively. For the straight non-circular cross-section, the strain contour is uniform; however, for the other two cases, the strain varies through the height due to the non-uniform geometry. Figure 12 shows the overall response of the stems due to external loading. As seen in Fig. 12, the "engineering strains (d/L)" for all cases (corresponding to models (A)–(C) in Fig. 11) are similar; however, there is a larger variation in the local axial strain responses among the specimens, which as an example is shown by the strains at the center location on the free lateral surface of the stem. These slight variations in the tensile responses from the geometries of the stems can influence the material parameter characterizations.

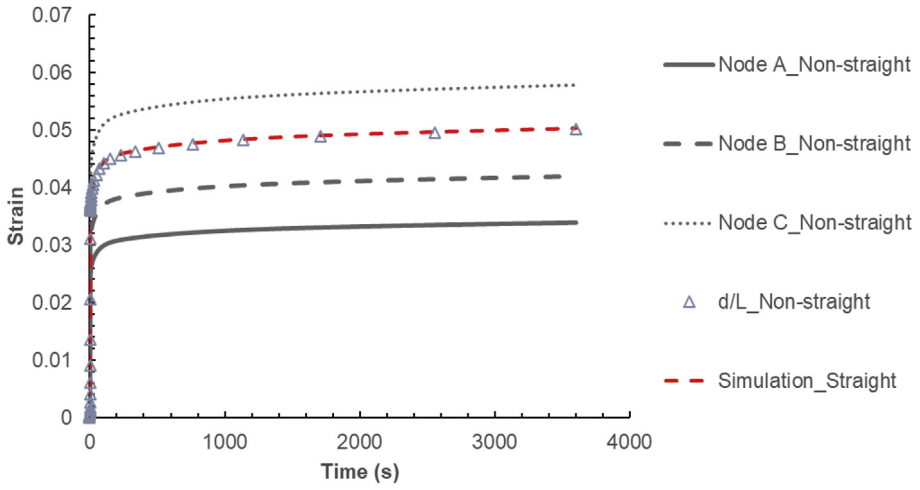

(a)

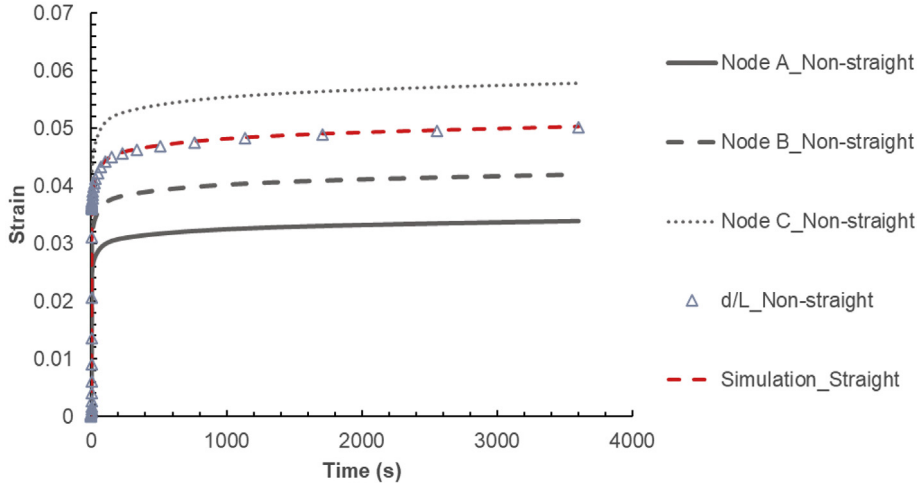

(b)

Fig. 8 – Overall response during creep compression of a "real" stem with axial misalignment through the height (non-straight) with a) free-sliding boundary conditions, b) fixed boundary conditions.

3.7. *Simulating bending responses*

As previously mentioned, a prominent failure mode in plant lodging is associated with bending of the stems (see Fig. 13). We thus analyze the creep bending response of a sorghum stem during a 4-point bending test by incorporating tension and compression properties we calibrated from the previous sections. In other words, for the region under compression (top), we assigned viscoelastic and elastic properties to the pith and rind, respectively; however, for the region under tension (bottom), we used viscoelastic properties for both pith and rind (See Fig. 13b, d, f). As in the previous section we consider three different geometries: a non-circular straight cylinder (Fig. 13a), a non-circular cylinder with a slight curve through the height (Fig. 13c), and a non-circular cylinder with two slight curves through the height (Fig. 13e). These figures show the longitudinal strain contour through the stem. The applied force is calibrated through FE analysis in such a way that the corresponding stress in the rind in the tension region correlates with the same stress level as the rind in the uniaxial tensile testing we have discussed before. Figure 14 also shows the longitudinal strain response of the stem due to creep bending at two different regions (Nodes A-F) for three different geometries

Table 3 – Instantaneous moduli and time-dependent parameters of sorghum pith under creep compression (E_1 to E_5 are time-dependent parameters to be used in a viscoelastic material model).

i	τ_i(s)	E_i (MPa)
0	–	20.0
1	5	95.4
2	50	53.2
3	500	141.4
4	5000	499.5
5	50,000	2.2

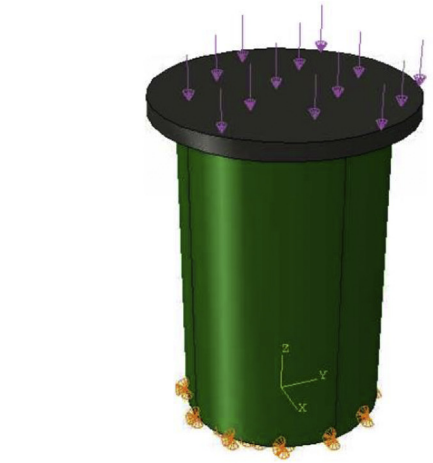

(a)

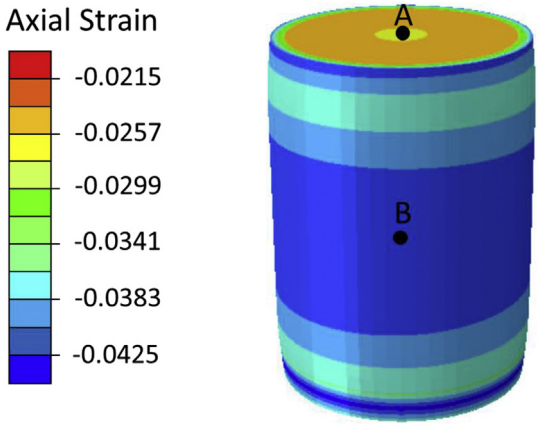

(b)

Fig. 9 – (a) Loading condition for the stem during compression creep (b) Axial strain contour plot of a stem undergoing compression creep loading, assuming the pith as viscoelastic material and the rind as a linear elastic material with a modulus of 325 MPa and fixed boundary conditions at time t = 1000 s.

Table 4 – Instantaneous moduli and time-dependent parameters of sorghum pith under creep tensile loading (E_1 to E_5 are time-dependent parameters to be used in a viscoelastic material model).

i	τ_i(s)	E_i (MPa)
0	–	20.0
1	5	16.02
2	50	30.3
3	500	66.28
4	5000	29.73
5	50,000	4.602

(non-circular straight cylinder, non-circular cylinder with a slight curve, and non-circular cylinder with two slight curves). We can see that at nodes C and E (compression locations), the longitudinal strain variation is 38% for the stem with a slight curve and 100% for the stem with two slight curves, as compared to straight stem (node A) (percent difference). This difference for nodes D and F (tension regions) is 39% for the stem with a slight curve and 9.4% a stem with two slight curves, as compared to the straight stem (node B).

4. Discussion

In this study, we investigated the effects of boundary conditions and geometric variations on the overall creep behavior of the sorghum stems to examine the influence of these variables on the experimental data, which were used to calibrate material parameters. In terms of geometric variations typically found in sorghum stems, we can conclude that cross-sectional variations and curvatures along the longitudinal axis (whether they are straight or not) do not change the overall engineering compressive and tensile strain. However, these geometric variations result in large local differences in stresses and strains. For instance, in a sorghum stem misaligned through the height (non-straight), bending will occur when applying uniaxial compression loading. For compression loading, deviations in strains from straight cylinders are higher while using a free sliding boundary condition which is

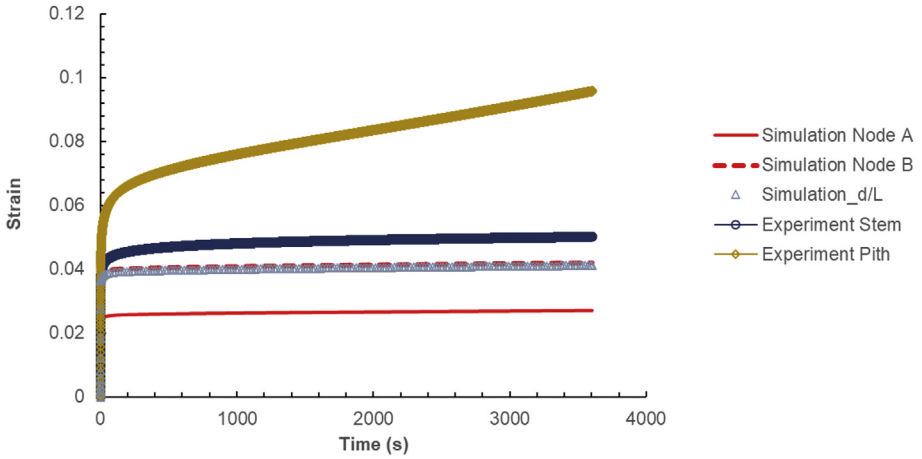

Fig. 10 – Overall response of a stem under creep compression loading of 1.9 MPa, assuming the pith as viscoelastic material and rind as a linear elastic material with a modulus of 325 MPa with fixed boundary conditions.

Table 5 – Instantaneous moduli and time-dependent parameters of sorghum rind under creep tensile loading (E_1 to E_5 are time-dependent parameters to be used in a viscoelastic material model).

i	τ_i(s)	E_i (MPa)
0	–	580
1	5	606
2	50	751
3	500	1118
4	5000	625
5	50,000	1062

up to 23% and 21% (percent difference) in compression and tension regions, as compared to the straight sample. In terms of tensile responses, a slight curve (by 3° with respect to the longitudinal axis) changes the strain response up to 21% in the middle surface, and two slight curves through the height of the sample can change the response up to 11% (percent differences). Similarly, in bending, a slight curve through the height changes the strain response in the middle cross-section up to 39% in tension regions and 38% in compression regions. Having two slight curves through the height changes the strain response up to 9.4% in tension regions and 100% in compression regions (percent differences). This localized strain is important for predicting failure of the stem. From these simulations, we can conclude that using the 'engineering stress–strain' measures under tension and compression tests can only give us 'average' mechanical properties of the stems. The localized stress/strain that occurs in the specimens can potentially lead to localized failures at local stresses/strains that are much larger than those detected (i.e., measured) from the average mechanical responses of the stems. Under bending, the localized strain (and stress) responses are sensitive to the geometrical parameters of the stems, which can significantly affect the calibrated material parameters. Thus, we conclude that to properly extract the material parameters from the standard mechanical testing procedures, i.e., compression, tension, and bending, it is necessary to model the geometry of the samples properly. More precise representations of the geometry can be obtained from optical image of the tested specimens, as implemented in this study.

In terms of boundary conditions, we observed that for a non-circular straight cross-section, the free sliding boundary condition does not affect the strain response but the fixed boundary condition does affect the local strain response, as compared to a circular cross-section. For non-straight samples, both boundary conditions influence the local strain response. In all cases, the "engineering strain" that we measure in the experiment matches the overall longitudinal strain in the simulations (d/L). However, strain is a field variable, and hence there are local variations in the strain that vary depending on the boundary conditions. For a non-straight stem, the free sliding boundary condition could change the

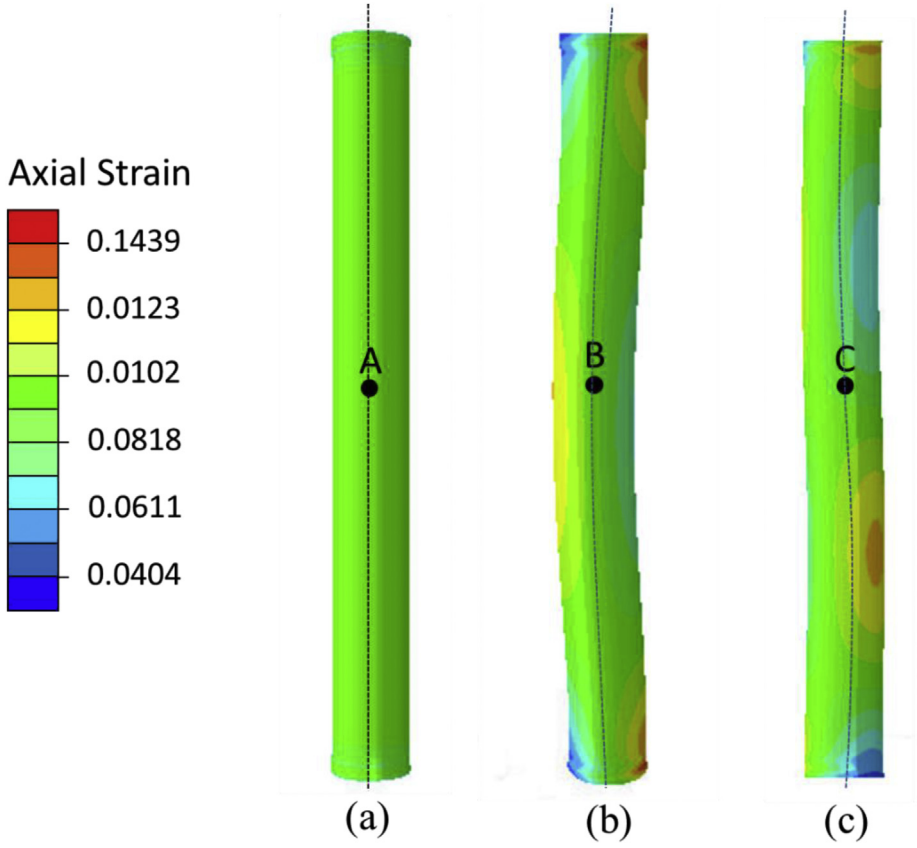

Fig. 11 – Axial strain contour plot of a stem undergoing tensile creep loading, assuming the pith and rind as viscoelastic materials with fixed boundary conditions at time t = 1000 s for a) perfect non-circular cylinder, b) a non-circular cylinder with a curve through the height, and c) a non-circular cylinder with two curves through the height.

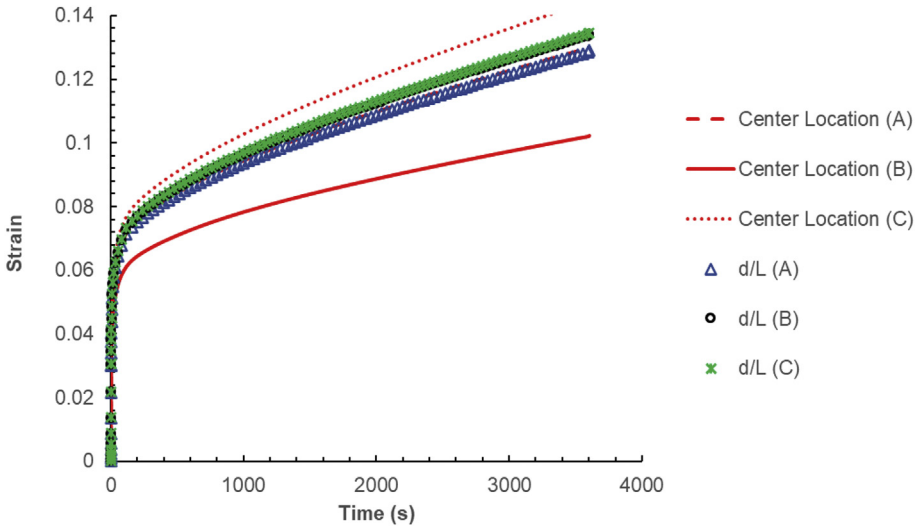

Fig. 12 – Overall response of the stem under creep tensile loading of 1.1 MPa for cases a-c (from Fig. 9).

compressive responses up to 0.2% at the top surface while this difference is up to 33% for the fixed boundary condition compared to straight stem. While in the actual experiments, the boundary condition on the top and bottom surfaces of the specimen is somewhere between the free sliding and fully constrained limits, it is very challenging (if not impossible) to determine the exact "correct" boundary condition in the experiment. This issue might have consequences in determining the overall mechanical properties of the stems.

We also studied the overall tensile, compressive, and bending response of the stem, considering the pith and rind properties individually. Based on the compressive responses, we found that although the rind supports the majority of the load and does not creep significantly itself, the pith does, and hence,

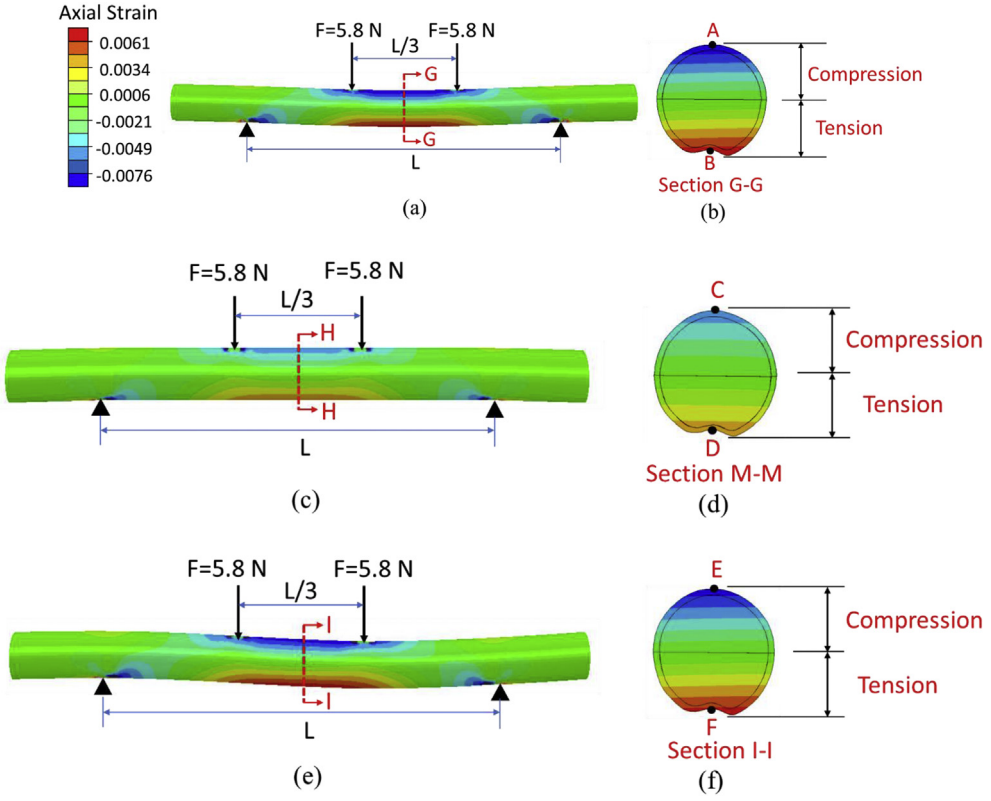

Fig. 13 – Longitudinal (axial) strain contour of the stem under creep bending loading at t = 1000 s: a) perfect non-circular straight cylinder, b) cross-section for non-circular straight cylinder, c) non-circular cylinder with a slight curve through the height, d) cross-section for non-circular cylinder with a slight curve, e) a non-circular cylinder with two curves through the height, and f) cross-section for non-circular cylinder with two curves through the height.

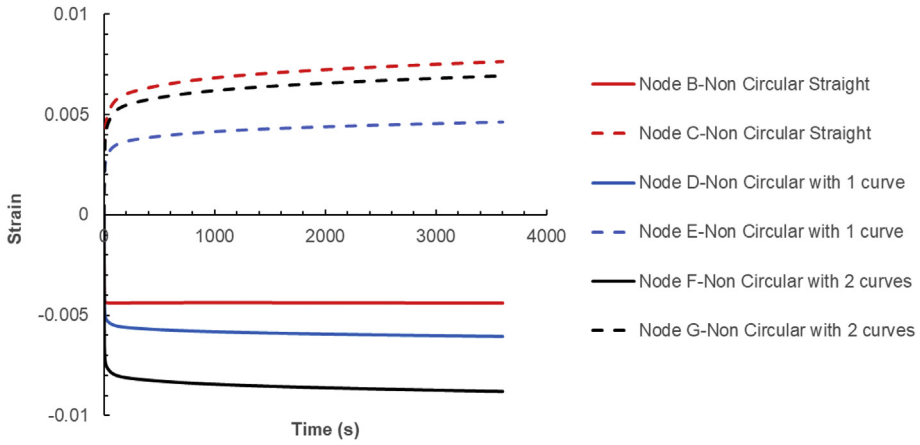

Fig. 14 – Overall response of the stem under creep bending loading at nodes A through F.

we get overall creep in the stem. Even though the applied load is constant, the resulting stress in the pith and rind evolves in time due to the creep of the pith and to maintain the equilibrium condition. Therefore, assuming the rind as an elastic component seems to be a reasonable approximation (recall that compression experiments on the rind are cumbersome or impossible). The bending results indicate that by incorporating tensile and compressive creep properties for the corresponding rind and pith constituents, an overall creep response for the stem can be predicted, in which the predicted longitudinal strain as a function of position could be used to predict stem lodging.

5. Limitations

As we are testing fresh samples, there is a possibility of water loss during the specimen preparation prior to testing. To minimize water loss, we ensured that all samples were tested within 6 h from cutting them from the plants. However, it is possible that some water loss did occur in this 6-h window. Future studies should include weighing the specimens immediately after cutting them from the plants and immediately prior to each mechanical test.

The creep tests were performed for 1 h, which is a relatively short term. This short-term test was performed since we tested fresh samples, and longer-term creep tests (e.g., days) may cause water loss from evaporation. Future studies may consider long-term creep tests of fresh stems, which is also important in accounting for other physical process such as water migration during testing.

6. Conclusions

In this study, we conducted experimental creep tests on sorghum stems, piths, and rinds. We also investigated the biomechanical response of sorghum stem through finite element analysis to analyze the effects of geometric irregularities in plants (deviations in cross-sectional and longitudinal shape from perfect circular cylinders), as well as any potential artifacts associated with boundary conditions during mechanical testing. Through finite element simulations, we show that the typical differences found in cross-sectional shapes of stems and curvatures through the stem height (e.g., a 3-degree deviation from straight cylinders) have a negligible influence on the average tension and compression responses of the stem during mechanical testing. However, finite element analysis indicated that these variations do alter the local strain at specific key locations relative to a perfect circular cylinder (up to 33% and 23% for fixed and free sliding boundary conditions, respectively). Failure may occur prematurely during testing due to these effects, as stresses will develop that readily exceed the strength of the plant locally prior to what is measured globally. We also determined that although the rind supports the majority of the load and does not creep significantly itself, the pith does, and hence we get overall creep in the stem. Overall, even though geometrical irregularities in sorghum stems present challenges, mechanical testing is still useful in extracting overall (average) mechanical responses of the stems under compression, tension, and bending. Finite element models with realistic stem geometries can improve the fidelity in extracting mechanical properties in these tests. In the future, full-field measurement testing and/or localized testing, e.g., indentation, may prove useful in providing more accurate measurements of the biomechanical properties of stems. The full-field measurement and/or localized testing will require the corresponding testing simulation (digital twin or virtual testing approach) to properly extract material properties.

Declaration of competing interest

The authors declare that they have no known competing financial interests or personal relationships that could have appeared to influence the work reported in this paper.

Acknowledgments

This research is sponsored by the US National Science Foundation under grant CMMI-1761015. We provide a special thanks to Qing Li who grew the sorghum for biomechanical testing. We also thank Dr. Scott A. Finlayson for his valuable

advice during this project. The finite element analyses were conducted at the Texas A&M's High-Performance Research Computing Center. This support is gratefully acknowledged.

Appendix A

This Appendix discusses simulation results for investigating the influence of material anisotropy on uniaxial loading and bending of plant stems, following typical experimental tests. The stems are modeled as a composite material having rind (outer layer) and pith (inner core) tissues. For each uniaxial compression and bending case, three material behaviors were considered. The first two cases (Case (a) and Case (b)) consider both pith and rind as transversely isotropic materials. As we pointed out that we were limited in obtaining multi-axial material properties for the sorghum stems, we referred to (Bozorg et al., 2014) and (Kaplan et al., 2019) in determining the transversely isotropic properties of the tissues. Kaplan et al. (2019) discussed that for the studied *Arabidopsis* cell walls, the transverse modulus is stiffer than the axial modulus (315 ± 46 kPa for axial walls compared to 488 ± 104 kPa for transverse walls), while Bozorg et al. (2014) in their simulation of plant cell wall used the transverse modulus to be half of the axial modulus (12 GPa for the axial modulus and 6 GPa for the transverse modulus). In our simulations we considered the transverse modulus to be twice of the axial modulus for Case (a), while for Case (b) we considered the transverse modulus to be half of the axial modulus. The material properties used for the pith and rind for all cases are given in Table A.1. The third case (Case (c)) considers both pith and rind as linear elastic isotropic materials, with properties are given in Table A.1. In this simulation, we only consider linear elastic behaviors due to a lack of studies regarding multi-axial viscoelastic properties of the tissues.

We first simulated uniaxial compression loading to mimic the compression experiment. Figure A.1 shows the axial force-displacement from the three cases, which indicated that considering an anisotropic material model for both rind and pith does not significantly alter the overall force-displacement responses of the stems. From the axial force-displacement responses, the axial stress and strain are constructed to determine the axial properties of the stem. The corresponding contour plots for the axial displacement, axial stress, and axial strain for the three cases are given in Figure A.2. From this simulation, we can conclude that when the transverse modulus is stiffer than the axial modulus, the responses are similar to the ones of the isotropic material. In Case (b), the soft lateral modulus leads to more pronounced bulging.

We then modeled 4-point bending. Figure A.3 shows the lateral force-displacement from three cases, which indicated that considering an anisotropic material model for pith and rind does not significantly change the overall behavior of the stem. Figure A.4 also shows the contour plot for the axial displacement, axial stress, and axial strain. Based on this simulation we can see that when the transverse modulus is either softer or stiffer than the axial modulus, the overall responses are comparable to the isotropic material.

Table A.1 – Material properties of pith and rind for isotropic and anisotropic cases

Property	Component	Elastic Modulus (Axial) (MPa)	Elastic Modulus (Transverse) (MPa)	Shear Modulus (Axial) (MPa)	Shear Modulus (Axial) (MPa)	Poisson's Ratio
Isotropic	Rind	325	–	–	–	0.25
	Pith	20	–	–	–	0.25
Anisotropic (case a)	Rind	325	650	130	260	0.25
	Pith	20	40	8	16	0.25
Anisotropic (case b)	Rind	325	162.5	130	65	0.25
	Pith	20	10	8	16	0.25

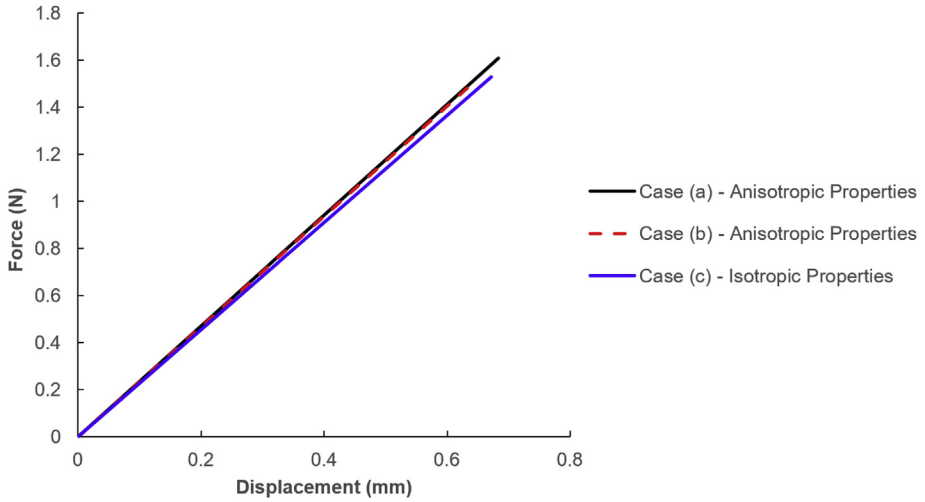

Fig. A1 – Uniaxial force-displacement from the compression simulations.

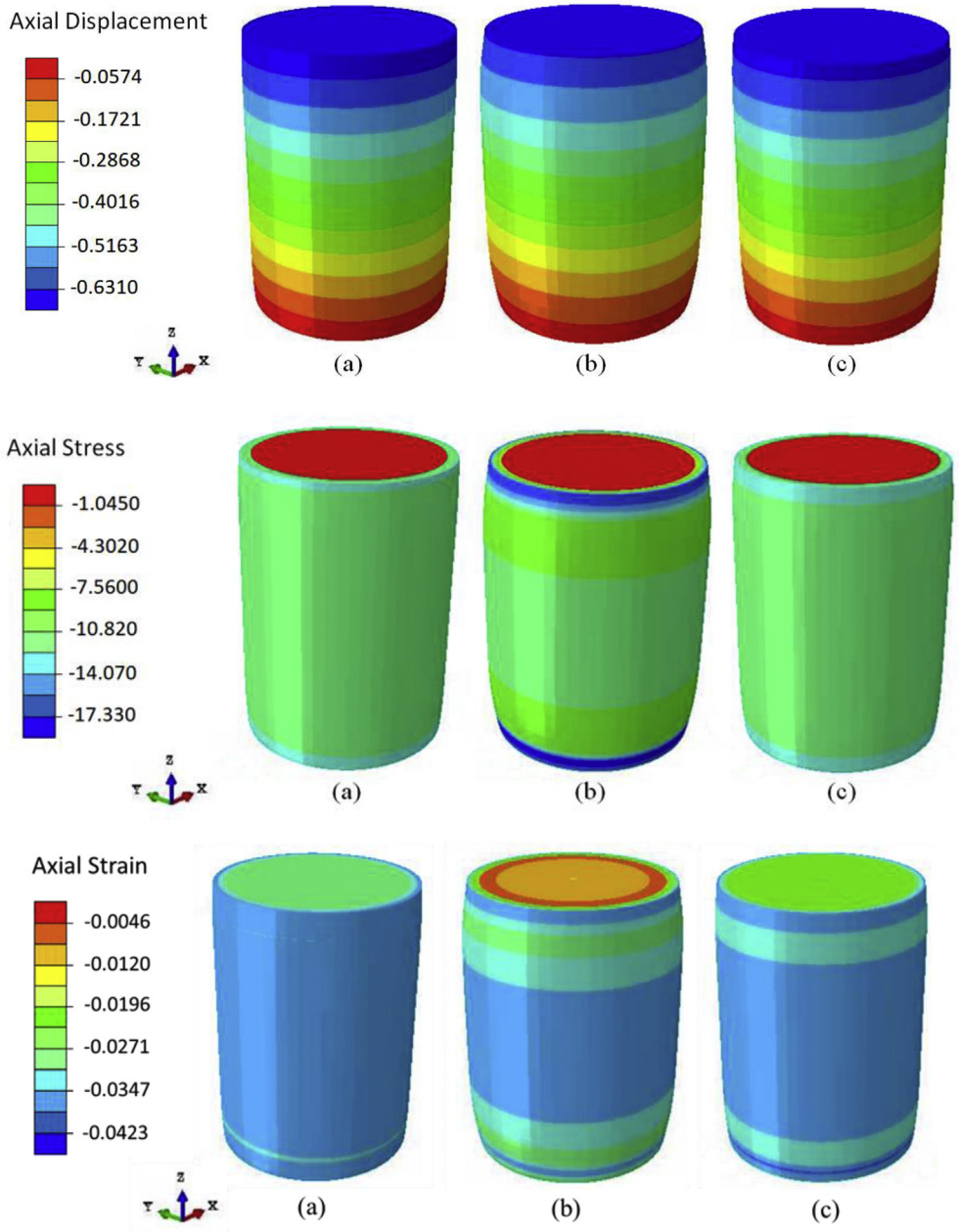

Fig. A.2 – Contour plots of axial displacement (in mm), axial stress (in MPa), and axial strain from the three cases.

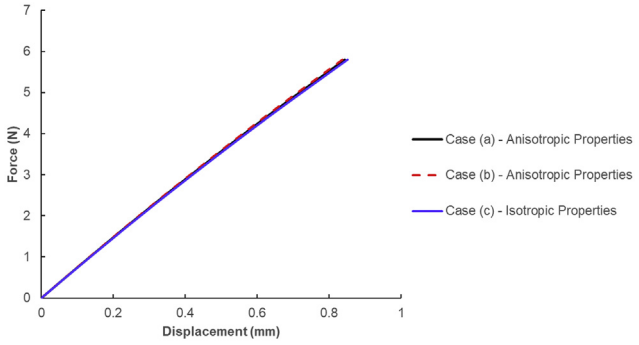

Fig. A3 – Lateral force-displacement from 4-point bending simulations.

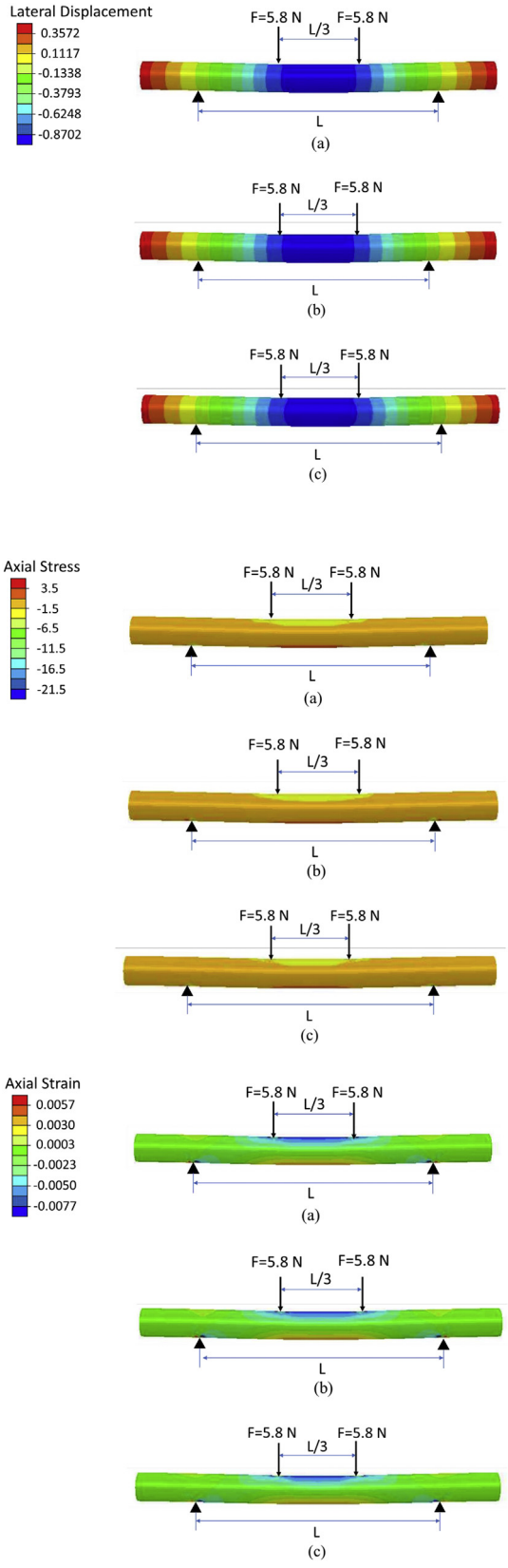

Fig. A.4 – Contour plots of lateral displacement (in mm), axial stress (in MPa), and axial strain from the three cases.

REFERENCES

Al-Zube, L. A., Robertson, D. J., Edwards, J. N., Sun, W., & Cook, D. D. (2017). Measuring the compressive modulus of elasticity of pith-filled plant stems. *Plant Methods, 13*(1), 99.

Al-Zube, L. A., Sun, W., Robertson, D., & Cook, D. D. (2018). The elastic modulus for maize stems. *Plant Methods, 14*(1), 11.

Alméras, T., Gril, J., & Costes, E. (2002). Bending of apricot tree branches under the weight of axillary growth: Test of a mechanical model with experimental data. *Trees, 16*(1), 5–15.

Berry, P., Sterling, M., Spink, J., Baker, C., Sylvester-Bradley, R., Mooney, S., … Ennos, A. (2004). Understanding and reducing lodging in cereals. *Advances in Agronomy, 84*(4), 215–269.

Boubakar, M., Vang, L., Trivaudey, F., & Perreux, D. (2003). A meso–macro finite element modelling of laminate structures: Part II: Time-dependent behaviour. *Composite Structures, 60*(3), 275–305.

Bozorg, B., Krupinski, P., & Jönsson, H. (2014). Stress and strain provide positional and directional cues in development. *PLoS Computational Biology, 10*(1), Article e1003410.

Cisse, O., Placet, V., Guicheret-Retel, V., Trivaudey, F., & Boubakar, M. L. (2015). Creep behaviour of single hemp fibres. Part I: Viscoelastic properties and their scattering under constant climate. *Journal of Materials Science, 50*(4), 1996–2006.

De Tommasi, D., Puglisi, G., & Saccomandi, G. (2006). A micromechanics-based model for the Mullins effect. *Journal of Rheology, 50*(4), 495–512.

Edelmann, H. G., & Köhler, K. (1995). Auxin increases elastic wall-properties in rye coleoptiles: Implications for the mechanism of wall loosening. *Physiologia Plantarum, 93*(1), 85–92.

Gomez, F. E., Carvalho, G., Shi, F., Muliana, A. H., & Rooney, W. L. (2018a). High throughput phenotyping of morpho-anatomical stem properties using X-ray computed tomography in sorghum. *Plant Methods, 14*(1), 59.

Gomez, F. E., Muliana, A. H., Niklas, K. J., & Rooney, W. L. (2017). Identifying morphological and mechanical traits associated with stem lodging in bioenergy sorghum (Sorghum bicolor). *BioEnergy Research, 10*(3), 635–647.

Gomez, F. E., Muliana, A. H., & Rooney, W. L. (2018b). Predicting stem strength in diverse bioenergy sorghum genotypes. *Crop Science, 58*(2), 739–751.

Hirano, K., Ordonio, R. L., & Matsuoka, M. (2017). Engineering the lodging resistance mechanism of post-Green Revolution rice to meet future demands. *Proceedings of the Japan Academy, Series B, 93*(4), 220–233.

Kaplan, J., Torode, T., Daher, F. B., & Braybrook, S. (2019). On pectin methyl-esterification: Implications for in vitro and in vivo viscoelasticity. *bioRxiv*, 565614.

Kin, K., & Shim, K. (2010). *Comparison between tensile and compressive Young's modulus of structural size lumber. Paper presented at the World conference on timber engineering*. Riva del Garda, Italy.

Kutschera, U., & Briggs, W. R. (1987). Differential effect of auxin on in vivo extensibility of cortical cylinder and epidermis in pea internodes. *Plant Physiology, 84*(4), 1361–1366.

Kutschera, U., & Briggs, W. R. (1988). Growth, in vivo extensibility, and tissue tension in developing pea internodes. *Plant Physiology, 86*(1), 306–311.

Kutschera, U., & Schopfer, P. (1986). In-vivo measurement of cell-wall extensibility in maize coleoptiles: Effects of auxin and abscisic acid. *Planta, 169*(3), 437–442.

Lee, S., Zargar, O., Reiser, C., Li, Q., Muliana, A., Finlayson, S. A., & Pharr, M. (2020). Time-dependent mechanical behavior of sweet sorghum stems. *Journal of the Mechanical Behavior of Biomedical Materials*, 103731.

Lemloh, M.-L., Pohl, A., Zeiger, M., Bauer, P., Weiss, I. M., & Schneider, A. S. (2014). Structure-property relationships in mechanically stimulated Sorghum bicolor stalks. *Bioinspired Materials, 1*(1), 1–11.

Niu, L., Feng, S., Ding, W., & Li, G. (2016). Influence of speed and rainfall on large-scale wheat lodging from 2007 to 2014 in China. *PLoS One, 11*(7), Article e0157677.

Robertson, D. J., Julias, M., Lee, S. Y., & Cook, D. D. (2017). Maize stalk lodging: Morphological determinants of stalk strength. *Crop Science, 57*(2), 926–934.

Robertson, D. J., Smith, S. L., & Cook, D. D. (2015). On measuring the bending strength of septate grass stems. *American Journal of Botany, 102*(1), 5–11.

Sawant, S., & Muliana, A. (2008). A thermo-mechanical viscoelastic analysis of orthotropic materials. *Composite Structures, 83*(1), 61–72.

Shah, D. U., Reynolds, T. P., & Ramage, M. H. (2017). The strength of plants: Theory and experimental methods to measure the mechanical properties of stems. *Journal of Experimental Botany, 68*(16), 4497–4516.

Song, R., & Muliana, A. (2019). Modeling mechanical behaviors of plant stems undergoing microstructural changes. *Mechanics of Materials, 139*, 103175.

Stubbs, C. J., Baban, N. S., Robertson, D. J., Alzube, L., & Cook, D. D. (2018). Bending stress in plant stems: Models and assumptions. In *Plant biomechanics* (pp. 49–77). Springer.

Stubbs, C. J., Sun, W., & Cook, D. D. (2019). Measuring the transverse Young's modulus of maize rind and pith tissues. *Journal of Biomechanics, 84*, 113–120.

Suslov, D., & Verbelen, J. (2006). Cellulose orientation determines mechanical anisotropy in onion epidermis cell walls. *Journal of Experimental Botany, 57*(10), 2183–2192.

Wirawan, R., Sapuan, S., Robiah, Y., & Khalina, A. (2011). Elastic and viscoelastic properties of sugarcane bagasse-filled poly (vinyl chloride) composites. *Journal of Thermal Analysis and Calorimetry, 103*(3), 1047–1053.

Wright, C. T., Pryfogle, P. A., Stevens, N. A., Steffler, E. D., Hess, J. R., & Ulrich, T. H. (2005). Biomechanics of wheat/barley straw and corn stover. *Applied Biochemistry and Biotechnology, 121*(1–3), 5–19.

Yuan, Z., Muliana, A., & Rajagopal, K. (2020). Modeling deformation induced anisotropy of light-activated shape memory polymers. *International Journal of Non-linear Mechanics, 120*, 103376.

Zeng, X., Mooney, S. J., & Sturrock, C. J. (2015). Assessing the effect of fibre extraction processes on the strength of flax fibre reinforcement. *Composites Part A: Applied Science and Manufacturing, 70*, 1–7.

Zuber, M., Colbert, T., & Darrah, L. (1980). Effect of recurrent selection for crushing strength on several stalk components in maize 1. *Crop Science, 20*(6), 711–717.